PNAS RESEARCH ARTICLE | CHEMISTRY

# A DNA-based hydrogel for exosome separation and biomedical applications

Jianpu Tang[a,1], Xuemei Jia[a,1], Qian Li[a,1], Zhen Cui[a], Aiqi Liang[a], Bin Ke[b], Dayong Yang[a,2], and Chi Yao[a,2]

Edited by David Weitz, Harvard University, Cambridge, MA; received March 7, 2023; accepted June 4, 2023

**Exosomes (EXOs) have been proven as biomarkers for disease diagnosis and agents for therapeutics. Great challenge remains in the separation of EXOs with high-purity and low-damage from complex biological media, which is critical for the downstream applications. Herein, we report a DNA-based hydrogel to realize the specific and nondestructive separation of EXOs from complex biological media. The separated EXOs were directly utilized in the detection of human breast cancer in clinical samples, as well as applied in the therapeutics of myocardial infarction in rat models. The materials chemistry basis of this strategy involved the synthesis of ultralong DNA chains via an enzymatic amplification, and the formation of DNA hydrogels through complementary base-pairing. These ultralong DNA chains that contained polyvalent aptamers were able to recognize and bind with the receptors on EXOs, and the specific and efficient binding ensured the selective separation of EXOs from media into the further formed networked DNA hydrogel. Based on this DNA hydrogel, rationally designed optical modules were introduced for the detection of exosomal pathogenic microRNA, which achieved the classification of breast cancer patients versus healthy donors with 100% precision. Furthermore, the DNA hydrogel that contained mesenchymal stem cell–derived EXOs was proved with significant therapeutic efficacy in repairing infarcted myocardium of rat models. We envision that this DNA hydrogel–based bioseparation system is promising as a powerful biotechnology, which will promote the development of extracellular vesicles in nanobiomedicine.**

DNA nanotechnology | hydrogel | exosomes | nanobiomedicine

## Significance

Exosomes (EXOs) are a type of lipid bilayer vesicles with the diameter of 30 to 150 nm secreted by cells. It has been proved that EXOs play important roles in the regulation of physiological activities, and can be utilized as biomarkers for disease diagnosis or agents for therapeutics. However, great challenge remains in the separation of EXOs with high-purity and low-damage from complex biological media. Herein, we develop a DNA hydrogel–based separation technology, achieving the specific and nondestructive separation of EXOs from cell culture medium and serum. Furthermore, we design this DNA hydrogel to realize the detection of exosomal pathogenic microRNA in clinical serum samples and the treatment of the rat myocardial infarction model.

Exosomes (EXOs) have been proven to participate intercellular communication and regulate a series of physiological or pathological processes (1, 2). The separation and analysis of EXOs in complex systems is of great significance for the early diagnosis, pathogenesis analysis, and prognosis monitoring of major diseases (3–6). As a prerequisite of downstream bioanalytical and therapeutic applications, the efficient and nondestructive separation of EXOs from complex biological media is crucial (7). However, challenge still remains in the separation of EXOs with high-purity and low-damage from biological media, which is mainly because i) the sizes of EXOs are much smaller (usually 30 to 150 nm), and the densities of EXOs are similar to the medium; ii) there are a large number of nontarget vesicles in the medium; and iii) more notably, the structure and biological activity of EXOs are susceptible to external stimulation. Recently, several efficient technologies for EXO separation have been developed (7–9), including ultracentrifugation, sucrose-gradient centrifugation, polymer-based precipitation, and immunoaffinity enrichment. These technologies usually require a large volume of samples, specialized equipment, and complicated operation. In addition, some inevitable factors during separation, such as shear force and medium change, seriously influence the structural integrity and biological activity of EXOs. To fundamentally solve these problems, strategies of EXO separation based on better materials and technologies are urgently required.

DNA nanotechnology has been developed in the field of bioseparation in recent years (10, 11), which is mainly based on the specific recognition of DNA aptamers, a category of oligonucleotide sequences (12), toward target ligands. Due to the high affinity to specific ligands on biological particles (such as cells and EXOs), DNA aptamers have been developed to recognize target cells and cell-derived vesicles (12–18). Remarkably, by rationally integrating aptamer sequences into DNA network as a matter of hydrogel, a convenient, selective, and nondestructive separation toward specific cells such as stem cell, lymphocyte, and cancer cell has been achieved (15, 17, 19). The aptamers in DNA hydrogel are elaborately selected according to the biomarkers on the membrane of target cells. It is expected that, by selecting desired aptamer toward EXOs, the DNA hydrogel is promising for the separation of EXOs from complex biological samples.

Author contributions: J.T., X.J., D.Y., and C.Y. designed research; J.T., X.J., Q.L., Z.C., A.L., and B.K. performed research; B.K. contributed new reagents/analytic tools; J.T., X.J., Q.L., Z.C., A.L., D.Y., and C.Y. analyzed data; and J.T., Q.L., D.Y., and C.Y. wrote the paper.

The authors declare no competing interest.

This article is a PNAS Direct Submission.



[1]J.T., X.J., and Q.L. contributed equally to this work.

[2]To whom correspondence may be addressed. Email: dayong.yang@foxmail.com or chi_yao@foxmail.com.

This article contains supporting information online at https://www.pnas.org/lookup/suppl/doi:10.1073/pnas.2303822120/-/DCSupplemental.

Published July 3, 2023.

Herein, we report a DNA-based hydrogel to realize the specific and nondestructive separation of EXOs from complex biological media. The DNA hydrogel was constructed from ultralong single-stranded DNA (ssDNA) that was synthesized via double-rolling circle amplification (RCA) (20, 21). An aptamer that specifically recognized tetraspanin CD63 on EXOs (22–24), named AptCD63, was designed in the template of RCA, and thus polyvalent aptamers were produced. As a result, the obtained ultralong ssDNA possessed high affinity toward CD63-positive EXOs, achieving specific capture and efficient enrichment of EXOs in the further formed DNA hydrogel. We applied the DNA hydrogel in the selective separation of EXOs from biological media, such as cell culture medium and patient serum. The separated EXOs can be nondestructively released from hydrogel via enzymatic cleavage and strand-displacement. Further, as a demonstration of bioanalysis, we implemented the detection of exosomal pathogenic microRNA (miRNA) in clinical samples along with the separation process of tumor cell–derived EXOs. Moreover, as a demonstration of therapeutics, we applied the bone marrow stromal cell (BMSC)–derived EXOs separated by DNA hydrogel to the treatment of the rat myocardial infarction (MI) model.

## Results

**Design and Construction of DNA Hydrogel for EXO Separation.** The DNA hydrogel–based separation technology included three key steps: enzymatic amplification to synthesize two ultralong DNA chains, the pretreatment of medium by low-speed centrifugation, and the separation of EXOs by DNA hydrogel (Fig. 1). The two ultralong DNA chains (DNA-chain-1 and DNA-chain-2) were, respectively, produced by RCA using two circular DNA (circ-DNA) as templates (Fig. 1*A* and *SI Appendix*, Fig. S1 and Table S1). The complementary sequence of AptCD63 was integrated to circ-DNA-1, and thus DNA-chain-1 contained repeated sequences of AptCD63 (polyvalent AptCD63). The EXO-containing medium, such as cell culture medium and patient serum, was pretreated by low-speed centrifugation to remove cells and cell debris, during which the components with small size and low density remained in the supernatant, including EXOs, nontarget vesicles such as exomeres and high-density lipoprotein (HDL) (25). Upon adding DNA-chain-1 and gently shaking for 0.5 h at 37 °C, the EXOs in supernatant were anchored on DNA-chain-1 through the high affinity between AptCD63 and CD63 (Fig. 1*B*). Next, DNA-chain-2 was added into the system, and incubated for another 0.5 h at 37 °C. Through the 22-nt complementary sequences in DNA chains, DNA-chain-2 hybridized with DNA-chain-1 driven by hydrogen bond, forming DNA hydrogel. During the formation of DNA hydrogel, the captured EXOs were encapsulated in the hydrogel and separated from other components.

The formation of DNA hydrogel by the two DNA chains was first confirmed. The solutions of two DNA chains were mixed in a 1.5-mL tube, and shaken for 0.5 h at 37 °C; as a result, a bulk of DNA hydrogel formed (Fig. 2*A*). The rheology results showed that the storage modulus (G′, ~4 Pa) was higher than the loss modulus (G″, ~0.5 Pa), indicating the solid state and super-softness of DNA hydrogel (Fig. 2*B*). The porous microstructure of DNA hydrogel was important for the diffusion of EXOs in separation process. The images of scanning electron microscopy (SEM) and fluorescence microscopy showed the microscale three-dimensional (3D) porous structure of DNA hydrogel (Fig. 2 *C* and *D*). The results of mercury intrusion assay showed that the porosity of DNA hydrogel was 78.66%, and the size of pores in the hydrogel was larger than 100 nm, which facilitated the diffusion of EXOs in hydrogel (*SI Appendix*, Fig. S2).

For the construction and optimization of DNA hydrogel, BMSC-derived EXOs that were obtained by ultracentrifugation were employed as a demonstration. To verify the specific recognition of AptCD63 aptamer toward EXOs, EXOs were stained by red fluorescent dye CM-DiI, and AptCD63 was modified with green fluorophore FAM. After incubating EXOs with AptCD63 for 0.5 h, the colocalization of green fluorescence with red fluorescence was observed by fluorescence microscopy (Fig. 2*E* and *SI Appendix*, Fig. S3). As a control, noncorrelative ssDNA (NC) modified with FAM was incubated with EXOs. Pearson's

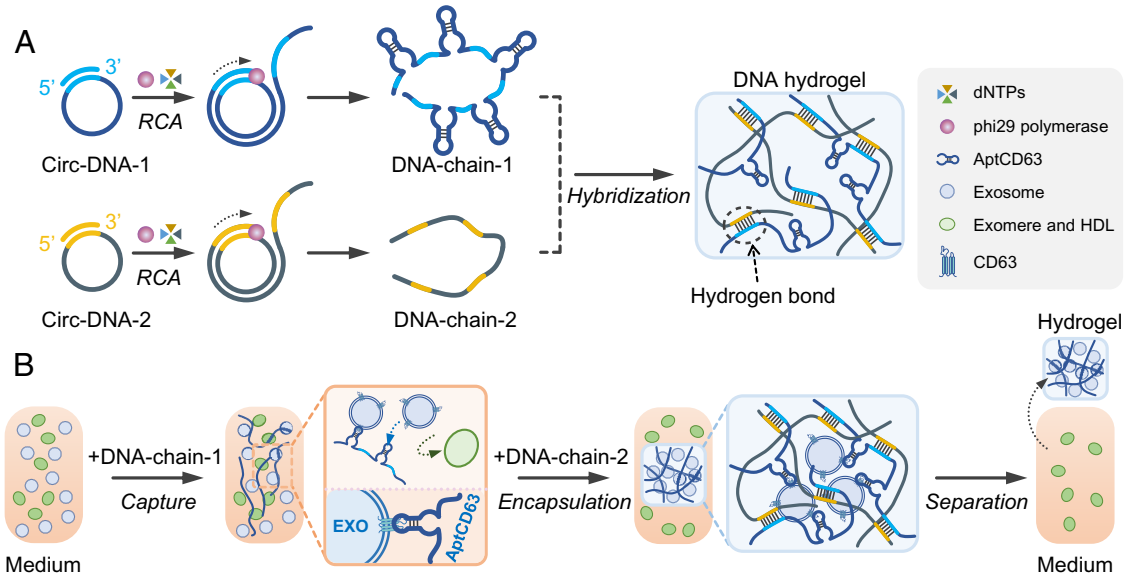


**Fig. 1.** Schematic illustration of DNA-based hydrogel for EXO separation. (*A*) Two types of ultralong DNA chains were synthesized by phi29 DNA polymerase-catalyzed RCA, and they were designed to hybridize with each other by complementary sequences to form DNA hydrogel. (*B*) The specific recognition of DNA aptamer (AptCD63) in DNA-chain-1 toward CD63 protein on EXOs to achieve the capture of EXOs; the hybridization between two DNA chains to encapsulate EXOs by forming DNA hydrogel, and thus achieve the separation of EXOs from biological medium. EXOs, exosomes; RCA, rolling circle amplification; dNTPs, deoxyribonucleoside triphosphates; HDL, high-density lipoprotein.

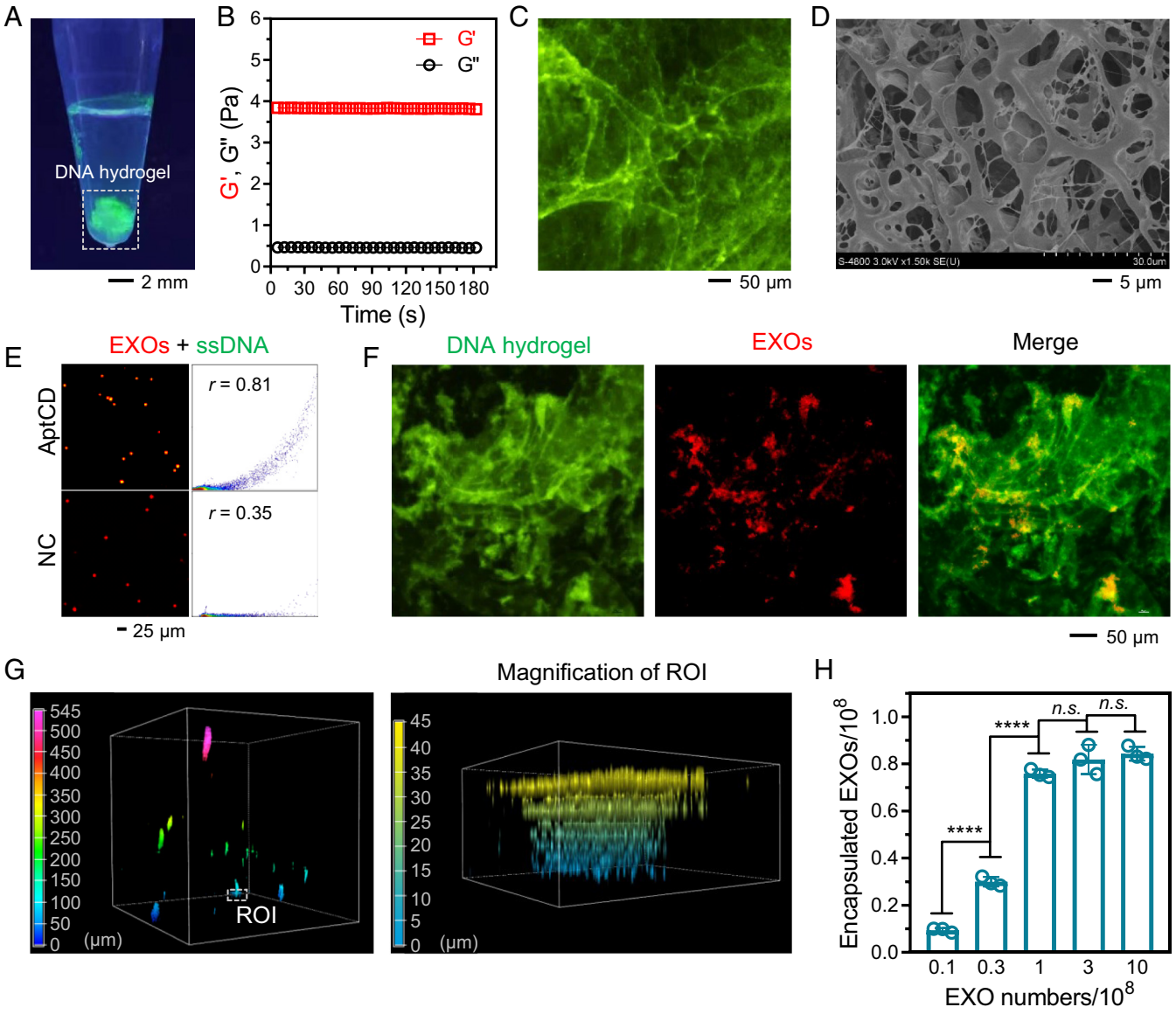


**Fig. 2.** Construction of DNA hydrogel for EXO separation. (*A*) Photograph of DNA hydrogel under ultraviolet light (UV, 302 nm). DNA hydrogel was stained by SYBR Green I. Rheology property (*B*), fluorescence microscopy image (*C*) and scanning electron microscopy image (*D*) of DNA hydrogel. (*E*) Fluorescent microscopy images (*Left*) of the specific binding between ssDNA (AptCD63, NC) and EXOs. AptCD63 and NC were modified with green fluorophore FAM. EXOs were stained with CM-DiI. Pearson's correlation coefficients (*Right*) were quantified to evaluate the coincidence of two fluorescence. (*F*) Fluorescence microscopy images to observe the EXOs encapsulated in DNA hydrogel. EXOs were stained with CM-DiI. DNA hydrogel was stained with SYBR Green I. (*G*) Three-dimensional stacking to observe the EXOs encapsulated in DNA hydrogel. ROI, region of interest. (*H*) Numbers of EXOs captured by DNA hydrogel in the media with different numbers of total EXOs. Results were presented as mean ± SD (n = 3 independent samples). ****$P < 0.0001$; *n.s.*, no significance, $P > 0.05$.

correlation coefficients were quantified as 0.81 (AptCD63) and 0.35 (NC), respectively, indicating the coincidence of AptCD63 and EXOs (Fig. 2*E*). These results demonstrated that AptCD63 was able to specifically recognize EXOs, which was an important prerequisite for the following EXO separation.

Next, the specific encapsulation of EXOs using DNA hydrogel was tested. The integration of AptCD63 sequence into DNA-chain-1 was verified using circular dichroism spectra (*SI Appendix*, Fig. S4), ensuring the specific recognition of DNA hydrogel toward EXOs. In fluorescence microscopy images, the fluorescence of EXOs colocalized well with that of DNA hydrogel (Fig. 2*F*). Fluorescence 3D stacking was further performed to observe the 3D spatial distribution of EXOs in DNA hydrogel. The images exhibited that EXOs were three-dimensionally distributed in the hydrogel as fluorescence dots, and the magnified region of interest showed that a large fluorescence dot contained a cluster of EXOs (Fig. 2*G*). These results indicated that EXOs were successfully encapsulated in the DNA hydrogel.

One of the important parameters of the separation technology was the capacity of DNA hydrogel to encapsulate EXOs. In the separation process, the volume ratio of DNA-chain-1 to DNA-chain-2 solution was 1:1. The numbers of encapsulated EXOs based on 50 μL DNA hydrogel were calculated. According to the linear relationship between EXO number and the fluorescence intensity of CM-DiI (*SI Appendix*, Fig. S5), the numbers of encapsulated EXOs were calculated by measuring the fluorescence intensity of the supernatant before and after separation. As shown in Fig. 2*H*, with initial EXO numbers increasing from $1 \times 10^7$ to $1 \times 10^8$, the numbers of encapsulated EXOs gradually increased, finally reaching a plateau with an encapsulation number of ~$7.6 \times 10^7$. These results indicated that the maximum encapsulation number to EXOs of 50 μL DNA hydrogel was $7.6 \times 10^7$.

**Controlled Release of EXOs from DNA Hydrogel.** The controlled release of captured EXOs from DNA hydrogel was explored. Taking the advantage of enzymatic degradation property of DNA, deoxyribonuclease I (DNase I) was used to degrade DNA hydrogel (26) (Fig. 3*A*). To study the process of enzymatic degradation, DNA hydrogel was incubated with different units of DNase I (0, 0.01, 0.1 and 1 U) at 37 °C, respectively. By measuring the DNA concentration in supernatant, we obtained the degradation rate of DNA hydrogel (*SI Appendix*, Fig. S6). The degradation rate significantly increased with the increase in DNase I concentration. Under the catalysis of 1 U DNase I, the degradation rate reached 100% at 60 min, much higher than that in 0.1 U (68.36%) and 0.01 U (43.22%) DNase I. During degradation, the cumulative release rate of EXOs was also monitored by measuring the

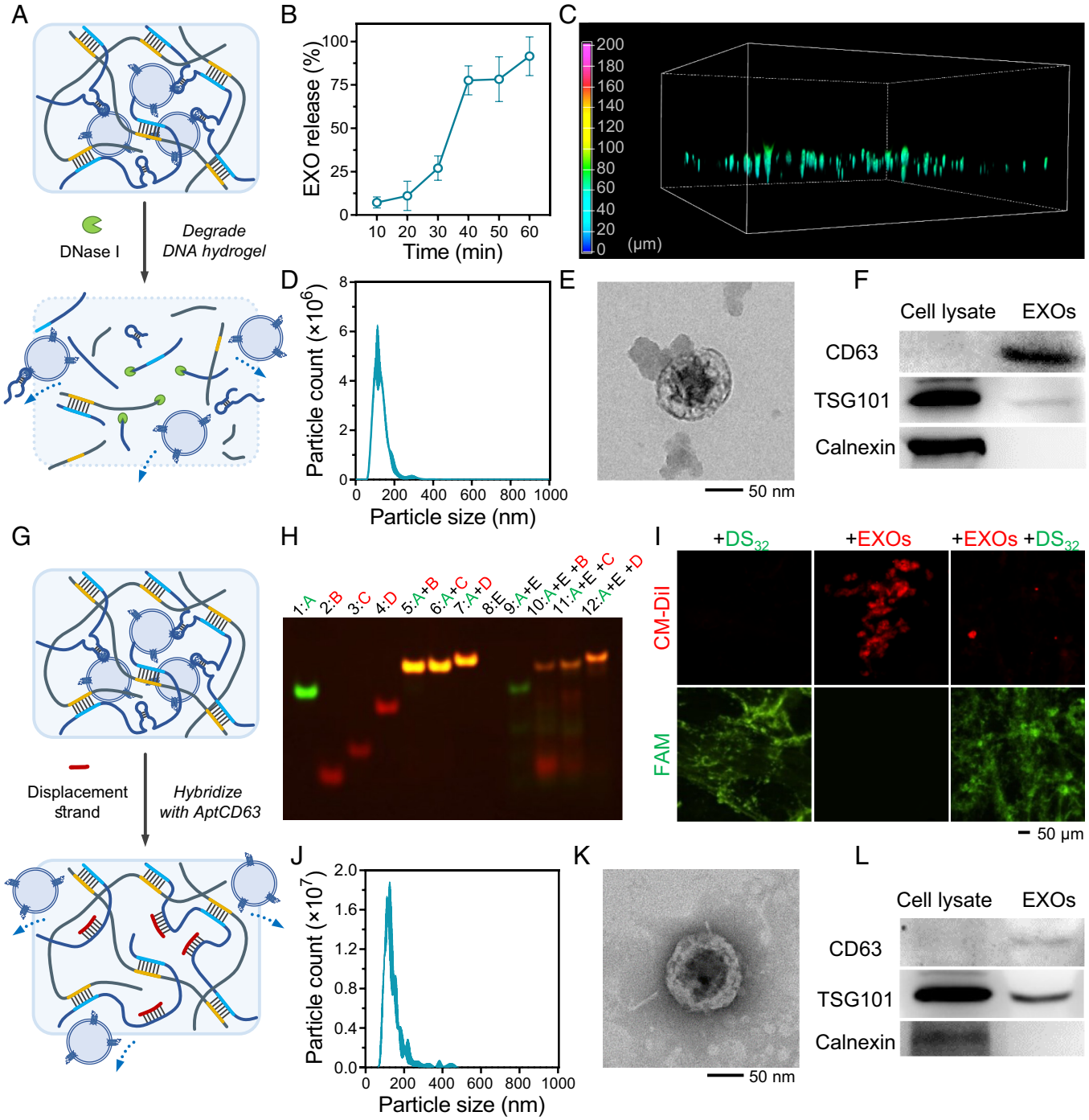


**Fig. 3.** Evaluation of two strategies of releasing EXOs from DNA hydrogel. (*A*) Schematic illustration of releasing EXOs from DNA hydrogel by enzymatic degradation. (*B*) Cumulative release rate of EXOs from DNA hydrogel over time under the degradation by 1 U DNase I. Results were presented as mean ± SD (n = 3 independent samples). (*C*) 3D stacking of the EXOs released in the degraded hydrogel. Nanoparticle tracking analysis (*D*) and TEM image (*E*) of the EXOs released via enzymatic degradation. (*F*) Representative bands of western blot assay for exosomal markers (CD63 and TSG101) and nonexosomal markers (calnexin). (*G*) Schematic illustration of releasing EXOs from DNA hydrogel through strand-displacement. (*H*) The 12% native polyacrylamide gel electrophoresis to verify the feasibility of strand-displacement. (*A*): FAM-labeled AptCD63; *B–D*: TAMRA-labeled $DS_{15}$, $DS_{20}$ and $DS_{32}$, respectively; *E*: EXOs. DS, displacement strand. (*I*) Fluorescence microscopy images to observe EXOs (stained by CM-DiI) and DNA hydrogel before and after adding $DS_{32}$ (labeled with FAM). Nanoparticle tracking analysis (*J*) and TEM image (*K*) of the EXOs released via strand-displacement. (*L*) Representative bands of western blot assay for exosomal markers (CD63 and TSG101) and nonexosomal markers (calnexin). Cell lysate was extracted from rat bone marrow mesenchymal stem cells.

fluorescence intensity of supernatant. When the concentration of DNase I was 0.1 U/mL, the cumulative release rate of EXOs from the DNA hydrogels with different concentrations (volume ratios of DNA hydrogel to buffer were 1:5, 1:10 and 1:15) at 60 min was all higher than 90% (Fig. 3*B* and *SI Appendix*, Fig. S7*A*); while the cumulative release rate of EXOs in the system without DNase I was only 6.54% (*SI Appendix*, Fig. S7*B*). The quick release of EXOs by enzymatic degradation allowed to efficiently obtain the dispersed EXOs for the experiments such as cell viability and cell proliferation tests. 3D stacking image showed the distribution of EXOs changing from 3D to single-layered, along with the degradation of hydrogel (Figs. 2*G* and 3*C*). In addition, considering that this DNA hydrogel would be utilized in biological media that contained nucleases, the release rate of EXOs was further monitored in 10% fetal bovine serum at 37 °C. The release rate of EXOs rapidly reached 54.99% in the first 4 h, and became slow after 8 h (*SI Appendix*, Fig. S8). These results demonstrated that enzymatic degradation achieved the efficiently controlled release of EXOs from DNA hydrogel.

To verify the structural integrity of the EXOs released via enzymatic degradation, the size, morphology, and biomarkers of the EXOs in degradation product were characterized (27). The hydrodynamic diameter of EXOs was ~110 nm measured by nanoparticle tracking analysis (Fig. 3*D* and *SI Appendix*, Fig. S9), and the saucer-shaped morphology of EXOs was observed in transmission electron microscopy (TEM) image (Fig. 3*E* and *SI Appendix*, Fig. S10), matching the typical structural characteristics of EXOs. The biomarkers of MCF-7-derived EXOs, CD63, and TSG101 (28), were detected by western blot assay. The nonexosomal markers, calnexin that was located in endoplasmic reticulum and Rab5 that was located in early endosome and plasma membrane, were detected in cell lysates, with much higher expression than EXOs (Fig. 3*F* and *SI Appendix*, Fig. S11). These results demonstrated that our DNA hydrogel–based technology was able to specifically separate EXOs, and the EXOs released via enzymatic degradation retained structural integrity.

Next, we designed another route, strand-displacement, to release EXOs, without disintegrating the DNA hydrogel. As mentioned above, the separation by our DNA hydrogel was based on the high affinity between AptCD63 and EXOs, which was closely related to the spatial configuration of AptCD63. Consequently, the nondestructive release of EXOs by changing the spatial configuration of AptCD63 to reduce the affinity between AptCD63 and EXOs was achieved (Fig. 3*G*). Three displacement strands (DSs) with different base numbers were designed, including $DS_{15}$, $DS_{20}$, and $DS_{32}$ (*SI Appendix*, Table S1). In our design, the DSs were completely complementary to AptCD63 and used to displace the captured EXOs from DNA hydrogel through hybridizing with the AptCD63 sequences on DNA-chain-1. To verify the competition effect of strand-displacement, 12% polyacrylamide gel electrophoresis (PAGE) was executed. To visualize the location of AptCD63 and DSs, AptCD63 was labeled with FAM (green fluorescent dye), and DSs were labeled with TRMRA (red fluorescent dye). As shown in Fig. 3*H*, two types of fluorescence overlapped well after mixing AptCD63 with DSs (lines 5 to 7, yellow fluorescence), and the bands moved much slowly compared with AptCD63 (line 1) as well as single DS (lines 2 to 4), indicating that all the three DSs effectively hybridized with AptCD63. To simulate the competition process, AptCD63 was mixed with EXOs, and then incubated with different DSs. As the base numbers in DS increasing, the bands in lines 10 to 12 showed that red fluorescent smears (DS) faded, and the fluorescent intensity of yellow bands (AptCD63+DS) was enhanced, indicating that more AptCD63 strands were displaced by DS from EXOs, and $DS_{32}$ showed the most significant competition effect. Consequently, $DS_{32}$ was chosen as the displacement strand in the following experiments.

The release process of EXOs from DNA hydrogel by strand-displacement was monitored by fluorescence microscopy. Significant green fluorescence was observed on the DNA hydrogel that was incubated with FAM-labeled $DS_{32}$ (Fig. 3 *I*, *Left*), demonstrating the efficient hybridization of $DS_{32}$ with AptCD63 on DNA hydrogel. Then, the EXO-encapsulated DNA hydrogel was incubated with FAM-labeled $DS_{32}$. Compared with the group without $DS_{32}$ (Fig. 3 *I*, *Middle*), the red fluorescence of EXOs in hydrogel was significantly weakened (Fig. 3 *I*, *Right*), demonstrating that $DS_{32}$ successfully displaced EXOs from DNA hydrogel. To verify the structural integrity of the EXOs released through strand-displacement, the size, morphology, and biomarkers of the EXOs were characterized. The hydrodynamic diameter of EXOs was approximately 110 nm (Fig. 3*J*), and the morphology was saucer-shaped in TEM image (Fig. 3*K*), matching the typical structural characteristics of EXOs. Biomarkers CD63 and TSG101 were detected in the supernatant of release system by western blot; nonexosomal markers calnexin and Rab5 were detected in cell lysates (Fig. 3*L* and *SI Appendix*, Fig. S11). These results demonstrated that the EXOs released by strand-displacement remained structural integrity.

**Detection of Exosomal miRNA Using DNA Hydrogel.** Exosomal miRNA is a category of reliable and noninvasive biomarker for the early diagnosis of cancer (29–31). However, the low abundance in EXOs and the tedious process of extraction often limited the sensitivity of exosomal miRNA detection. In our separation technology, after adding DNA-chain-2, the EXOs captured by DNA-chain-1 can be efficiently enriched as the formation of DNA hydrogel, which achieved a high local concentration of EXOs and was beneficial to improve the sensitivity of miRNA detection; moreover, the DNA hydrogel can work as a framework for the integration of detection units, e.g., oligonucleotide molecular beacon (MB) and single probe (SP) that have been utilized in in situ detection of EXOs (32, 33), achieving high specificity and accuracy. The sequences of MB and SP were designed and integrated to DNA hydrogel to develop a detection method toward exosomal microRNA-21 (miR-21) detection, a biomarker of breast cancer (31). MB was a hairpin-structure DNA that was modified with a red fluorophore Cy3 at 5′ and a quencher (BHQ2) at 3′; SP was an ssDNA modified with FAM at 5′ (Fig. 4*A* and *SI Appendix*, Table S1). When MB was at hairpin state, the fluorescence of Cy3 was quenched by BHQ2. Both MB and SP were designed to hybridize with DNA-chain-1: MB hybridized with AptCD63 sequence, and SP hybridized with nonaptamer sequence on DNA-chain-1 (Fig. 4*A*). When both MB and SP hybridized with DNA-chain-1, the fluorescence of FAM on SP was quenched by BHQ2 on MB due to their closer distance.

After hybridizing with MB and SP, DNA-chain-1 was added into biological medium to capture EXOs. When AptCD63 recognized CD63 on EXOs, CD63 displaced MB from DNA-chain-1 due to the higher affinity toward AptCD63, and the green fluorescence of FAM was recovered due to the weakened quenching effect from BHQ2. When the displaced MB penetrated into EXOs, the sequence on the loop of MB recognized miR-21 and hybridize to form double-stranded structure, which resulted in the weakened quenching effect of BHQ2 to Cy3 and the recovery of red fluorescence of Cy3. Finally, DNA-chain-2 was added to form DNA hydrogel. The enrichment of EXOs by DNA hydrogel enhanced the fluorescence signals of FAM and Cy3, so that the signals were able to be detected by fluorescence microscopy. In

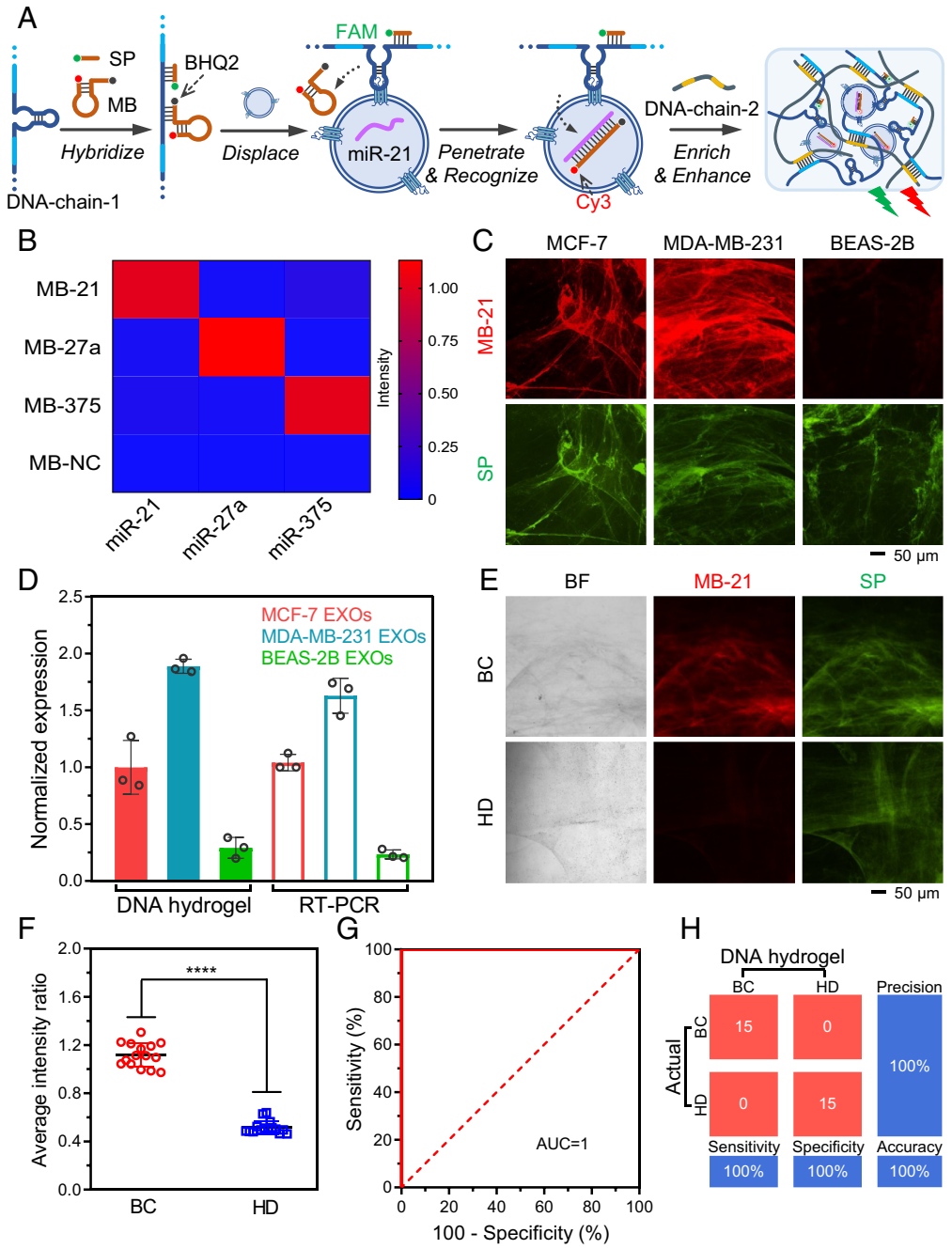


**Fig. 4.** Detection of exosomal miRNA in clinical samples of breast cancer patients using DNA hydrogel. (*A*) Schematic illustration of the detection of exosomal microRNA-21 (miR-21) using molecular beacon (MB) and single probe (SP). (*B*) Specificity of MBs toward varied miRNAs in an orthogonal assay. MB without complementary sequence (MB-NC) was used as negative control. (*C*) Fluorescence microscopy images showing the detection of exosomal miR-21 from varied cell line–derived EXOs by DNA hydrogel–based technology. MCF-7, human breast cancer cell; MDA-MB-231, human breast cancer cell; BEAS-2B, human bronchial epithelial cell. (*D*) Expression levels of exosomal miR-21 from varied cell line–derived EXOs measured by DNA hydrogel–based technology and RT-PCR, respectively. Results were presented as mean ± SD (n = 3 independent samples). (*E*) Fluorescent images of the DNA hydrogels to detect the exosomal miR-21 level in the serum of a breast cancer patient (BC) and a healthy donor (HD), respectively. (*F*) Scattered dot plots of the fluorescence ratio of DNA hydrogels after separating EXOs from the serum samples of HD (n = 15) and BC (n = 15). Results were presented as mean ± SD (n = 15 independent samples). ****$P < 0.0001$. (*G*) Receiver operating characteristic analysis to evaluate the performance of detection technology in breast cancer diagnosis. AUC, area under the curve. (*H*) Confusion matrix to summarize the discrimination performance of the DNA hydrogel–based detection technology between HD and BC.

particular, the green fluorescence was used as reference to minimize the influence of EXO concentration on detection accuracy by built-in correction (34). Consequently, the fluorescence intensity ratio of red to green was calculated to reflect the level of exosomal miR-21.

In our design, the specificity of MB was based on the complementary base pairing between MB and target miRNA, which was proved by 12% PAGE (*SI Appendix*, Fig. S12*A*). To verify the feasibility of fluorescence recovery, the fluorescence intensity of MB was measured with and without target miR-21, respectively. The fluorescence intensity increased 20.8 times in the presence of miR-21 (*SI Appendix*, Fig. S12*B*), demonstrating the efficient configuration transition of MB from hairpin to double helix, thus weakening the quenching effect of BHQ2 to Cy3. Then, three miRNAs (miR-21, miR-27a, miR-375) and the corresponding MBs (MB-21, MB-27a, MB-375) were used to study the specificity

of MB in an orthogonal assay, and MB with noncorrelated sequence (MB-NC) was used as a control. As shown in Fig. 4*B*, the fluorescence intensity of MBs was not affected by noncomplementary miRNAs, demonstrating the specificity of MB toward miRNA.

We next studied the feasibility of MB for the detection of miRNAs in the human breast cancer cell (MCF-7)–derived EXOs from cell culture medium. The penetration of MB into EXOs has been reported by the previous literatures (32, 35). We performed fluorescent colocalization experiment and proved the high penetration efficiency of MB-21 into MCF-7 EXOs by the well-overlapped fluorescence (*SI Appendix*, Fig. S13). To investigate the penetration process of MB-21 into EXOs, the fluorescence intensity of Cy3 was monitored after mixing MB-21 with MCF-7 EXOs (*SI Appendix*, Fig. S14). In the first 45 min, the intensity was gradually increased, indicating that the MB-21 was penetrating into the EXOs and recognizing miR-21; after 45 min, the intensity reached a plateau. In addition, MB-NC was used as a control to investigate the detection specificity of MB-21 toward exosomal miR-21, and only the group of MB-21 with MCF-7 EXOs showed the significant fluorescence of Cy3 (*SI Appendix*, Fig. S15). These results demonstrated the potential of MB-21 for specific detection of exosomal miR-21.

Two circ-DNAs of RCA were designed to produce new DNA chains (DNA-chain-1 and DNA-chain-2) for hybridization with MB-21 and SP, and the synthesis was proved by 12% PAGE (*SI Appendix*, Fig. S16). The time of RCA was optimized to obtain DNA chains that hybridized with more MB-21. When the time of RCA was 4 h, the fluorescence intensity of the MB-21 (without BHQ2) bound on hydrogel was the highest, and the fluorescence intensity of free MB-21 in supernatant was the lowest, indicating the highest hybridization efficiency of MB-21 with hydrogel (*SI Appendix*, Fig. S17). Next, the DNA chains produced by 4-h-RCA were utilized to hybridize with MB-21 and SP, and further formed DNA hydrogel. To ensure a high signal–noise (S/N) ratio of the detection, the ratio of MB-21 (with BHQ2) and SP added in the hydrogel was adjusted, and the corresponding S/N ratio by monitoring the two fluorescence of different hydrogels was calculated (*SI Appendix*, Fig. S18). After analysis, the optimal mole ratio of MB-21 to SP was determined as 1:0.6 (*SI Appendix*, Fig. S19). Finally, a fluorescent colocalization experiment was performed, demonstrating that the hydrogel formed by DNA-chain-1 and DNA-chain-2 was able to separate EXOs from cell culture medium (*SI Appendix*, Fig. S20).

Based on the above results, we applied DNA hydrogel–based separation technology to the detection of exosomal miR-21 in clinic samples of breast cancer patients (BCs). It has been proved that miR-21 was differentially expressed in normal tissues and cancer regions (36, 37). The feasibility of the semiquantitative detection of exosomal miR-21 from different cell lines was first investigated, including MCF-7, another human breast cancer cell (MDA-MB-231) and human bronchial epithelial cells (BEAS-2B). After treating the culture media from three cell lines by this technology, three DNA hydrogels encapsulating different EXOs were obtained and then observed by fluorescence microscopy (Fig. 4*C*). According to the microscopy images, the fluorescence intensity ratio of red to green was calculated to reflect the level of exosomal miR-21. As shown in Fig. 4*D*, the ratios of MCF-7 EXOs and MDA-MB-231 EXOs were approximately 3.42-fold and 6.47-fold higher than those of BEAS-2B EXOs, respectively. To evaluate the credibility of detection results, we also used RT-PCR as a standard to measure the expression levels of miR-21 in the three types of EXOs (Fig. 4*D*). The detection results from these two detection technologies showed a similar tendency, with a high correlation coefficient of 0.99 (*SI Appendix*, Fig. S21). These results demonstrated that our DNA hydrogel was potential for the semiquantitative detection of exosomal miR-21 with high accuracy.

To further evaluate the feasibility of the clinical diagnosis of breast cancer based on this DNA hydrogel, we measured the relative expression levels of miR-21 in 30 serum samples, from 15 BCs and 15 healthy donors (HDs). Each sample was treated to form DNA hydrogel. By fluorescent microscopy, two fluorescence images of DNA hydrogel (Fig. 4*E*) and the corresponding fluorescence intensity ratios of 30 samples (*SI Appendix*, Fig. S22) were obtained. As shown in Fig. 4*F*, the average ratio of the samples from BCs was 2.12-fold higher than that from HDs, indicating the significantly higher level of exosomal miR-21 in the samples of BCs. Receiver operating characteristic analysis showed the reliable discrimination of BC versus HD (area under the curve = 1, Fig. 4*G*); meanwhile, the confusion matrix showed 100% sensitivity and 100% specificity for the classification of BC versus HD by our DNA hydrogel–based separation technology (Fig. 4*H*). These results demonstrated the potential of our DNA hydrogel–based detection method in clinical diagnosis of breast cancer.

**Therapeutics toward MI Using DNA Hydrogel.** We next applied DNA hydrogel to the therapeutics toward MI. Previous studies have proven that BMSC-derived EXOs were able to effectively improve the hypoxic state of myocardia and repair infarcted cardiomyocytes (38, 39). To make EXOs play a better role of repair in the region of infarcted myocardia, the localized administration and efficient release of EXOs were crucial. DNA hydrogel was able to be enzymatically degraded to gradually release EXOs in serum-containing environment (*SI Appendix*, Fig. S8). The swelling degree of DNA hydrogel in fetal bovine serum was −51.97% in 8 h (*SI Appendix*, Fig. S23). The DNA hydrogel was also proved to be injectable due to its shear-thinning property (*SI Appendix*, Fig. S24), and showed stable storage modulus after 250 cycles under alternating strain between 1% and 500% (*SI Appendix*, Fig. S25), indicating excellent stability against shearing. On the other hand, the results of cholecystokinin octapeptide assay demonstrated the low cytotoxicity of DNA hydrogel, which was essential for the in vivo experiments (*SI Appendix*, Fig. S26). Consequently, our DNA hydrogel provided an ideal delivery method to achieve the localized administration and efficient release of EXOs. BMSC-derived EXOs were separated from culture medium of BMSCs and encapsulated in DNA hydrogel. To investigate whether these separated EXOs had the biological activity to protect cardiomyocytes from hypoxia damage, an in vitro hypoxia model was established by incubating rat cardiomyocytes (H9C2) under hypoxic condition (5% $O_2$) for 24 h. The results of living/dead cell assay showed that the numbers of dead cells in hypoxia group were significantly higher than those in the normoxia group, increasing from 7.16 to 24.09% (*SI Appendix*, Fig. S27), demonstrating the successful establishment of the in vitro hypoxia model. To verify the internalization of the EXOs released from DNA hydrogel by cardiomyocytes, the released EXOs were stained by CM-DiI and incubated with human cardiomyocytes (AC16) and rat cardiomyocytes (H9C2), respectively. With the increase in incubation time, the fluorescence intensity of CM-DiI increased significantly in the cytoplasm of cardiomyocytes (*SI Appendix*, Figs. S28 and S29), indicating the efficient internalization of EXOs. We then studied the influence of BMSC-derived EXOs on H9C2 cells under hypoxic condition. With the increase in the EXO concentration, the viability of H9C2 cells significantly increased, reaching 140.91% of that in normoxic control H9C2 cells at 30 μg/mL EXOs (*SI Appendix*, Fig. S30). Fluorescence microscopy images also proved that the number of proliferating H9C2 cells

(labeled by Alexa Fluor 488) gradually increased with increased EXO concentration (*SI Appendix*, Fig. S31). The protection effect toward hypoxia damage was further investigated at molecular level. Hypoxia inducible factor protein (HIF-1α) mediated the cellular response to hypoxia, which was overexpressed in cells under hypoxia condition (40). The results of western blot showed that the expression of HIF-1α in hypoxic H9C2 cells gradually decreased with increased EXO concentration; the HIF-1α level in hypoxic H9C2 cells treated with 10% EXOs was close to that in normoxic control H9C2 cells (*SI Appendix*, Fig. S32). These results demonstrated that the BMSC-derived EXOs separated by our DNA hydrogel possessed the biological activity of protecting cardiomyocytes from hypoxia damage.

To verify the sustained degradation of DNA hydrogel in vivo, GelRed-stained hydrogel was injected in the thoracic cavity of rat, and the change of fluorescence intensity was monitored. The fluorescence of GelRed on the 4th day decreased to 5.22% of that at the beginning (*SI Appendix*, Fig. S33). Based on these results, we applied the EXO-contained DNA hydrogel as a therapeutic agent in the rat MI model (Fig. 5*A*). The rat MI model was established by the ligation of the left anterior descending branch of coronary artery (LAD), and 100 μL DNA hydrogel encapsulating ~$2 \times 10^8$ BMSC-derived EXOs was injected onto the rat myocardium immediately following LAD ligation. At the 28-d end point, the heart function of rats was analyzed via echocardiography (Fig. 5*B*). Compared with the rats in normal group, the rats treated with PBS buffer showed significantly increased left ventricular internal dimensions (LVIDs) (*SI Appendix*, Fig. S34), as well as significantly decreased left ventricular ejection fraction (LVEF) (Fig. 5*C*) and left ventricular fraction shortening (LVFS) (Fig. 5*D*), indicating the severe ischemic necrosis of the myocardium. After being treated with EXO-contained hydrogel, the diastolic and

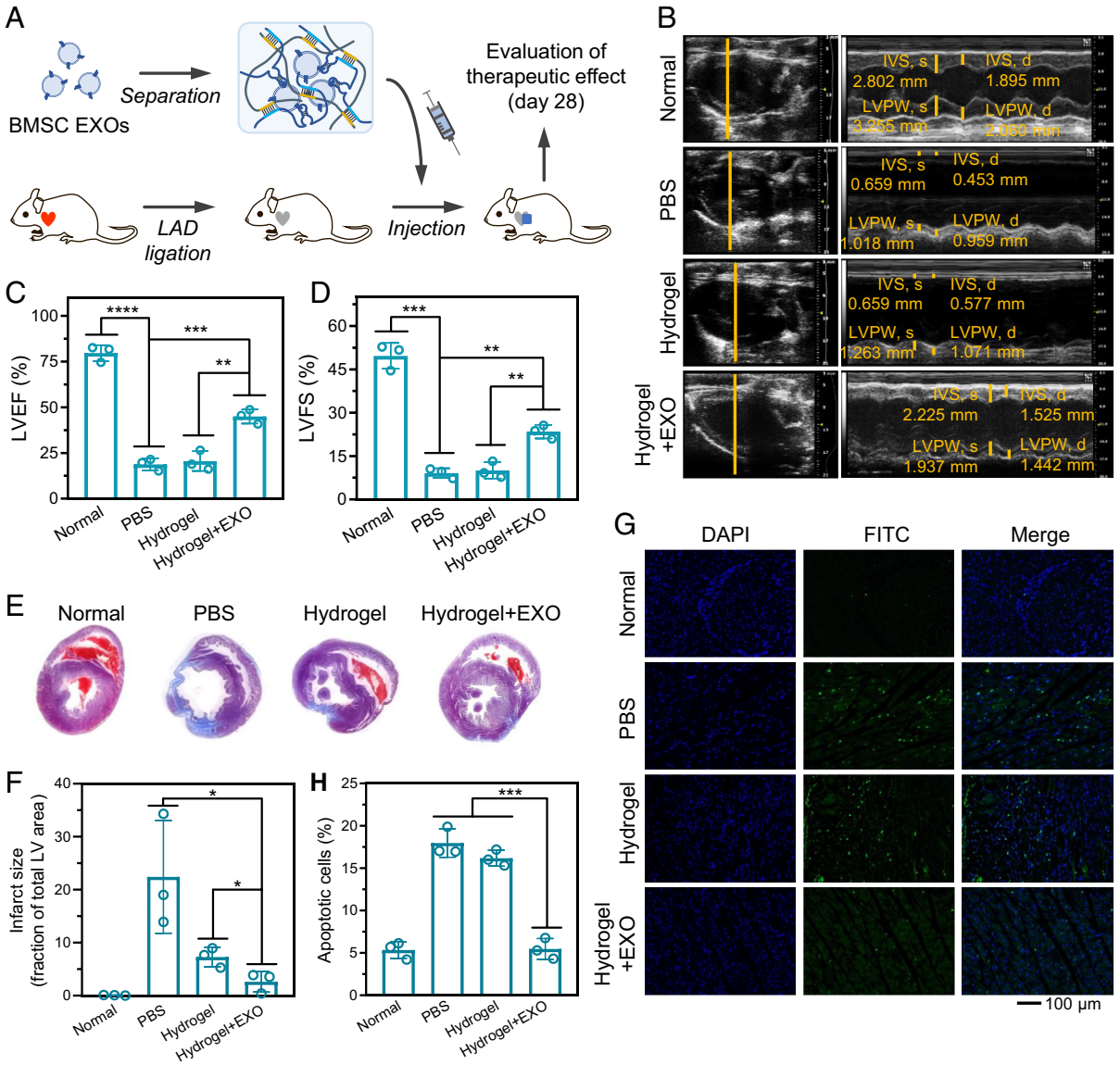


**Fig. 5.** Therapeutics of myocardial infarction (MI) in animal models using DNA hydrogel. (*A*) Schematic of DNA hydrogel–based therapeutics in the rat MI model. LAD, left anterior descending branch of coronary artery. (*B*) Representative M-mode echocardiogram images of the region marked by orange line for normal heart. The MI rats were divided into 3 groups, and treated with PBS, hydrogel, and hydrogel+EXO, respectively. IVS, interventricular septum. LVPW, left ventricular posterior wall. The left ventricular ejection fraction (LVEF) (*C*) and left ventricular fraction shortening (LVFS) (*D*) of rats after the treatment for 28 d. (*E*) Representative photographs of Masson's trichrome–stained paraffin sections of rat hearts. Dotted area (blue): collagen fiber. The MI rats were treated with PBS, hydrogel, and hydrogel+EXO. (*F*) Fractions of infarct size to total left ventricle (LV) area. (*G*) Representative fluorescent images of the paraffin sections of rat hearts to show the apoptosis cardiomyocytes (green) treated by TUNEL. (*H*) Percentages of apoptotic cells to total cells in the paraffin sections treated by TUNEL. Results were presented as mean ± SD (n = 3 independent samples). *$P < 0.05$; **$P < 0.01$; ***$P < 0.001$; ****$P < 0.0001$.

systolic LVIDs significantly decreased from 12.13 to 8.78% and from 11.21 to 7.10%, respectively; while LVEF and LVFS significantly increased from 18.80 to 45.01% and from 9.15 to 23.48%, respectively, demonstrating the significant therapeutic effect of improving the functions of the infarcted myocardium by our DNA hydrogel.

To further evaluate the therapeutic effect of DNA hydrogel, histology was performed at the 28-d end point. To quantitively analyze the cardiac collagen morphology, the paraffin sections of rat hearts were treated by Masson's trichrome staining, in which the areas of collagen fibrosis were stained blue (Fig. 5*E*). The results showed that the average fractions of the collagen fibrosis area to total left ventricle (LV) area were 0.07% (normal), 22.41% (PBS buffer), 7.30% (only DNA hydrogel) and 2.62% (DNA hydrogel containing BMSC-derived EXOs, hydrogel+EXO), respectively (Fig. 5*F*), indicating the significant therapeutic effect in blocking collagen fiber accumulation after treatment by our DNA hydrogel. On the other hand, to evaluate the apoptosis of myocardial cells, the paraffin sections of rat hearts were treated by terminal deoxynucleotidyl transferase-mediated dUTP nick-end labeling (TUNEL). The groups without EXO treatment (PBS and hydrogel) showed stronger green fluorescence in cell nuclei, indicating a higher level of apoptosis (Fig. 5*G*). In contrast, the apoptotic cells in the hydrogel+EXO group was 5.46% of total cells, which was significantly lower than that in the PBS group (17.96%) and hydrogel group (16.17%) (Fig. 5*H*). These results demonstrated that our DNA hydrogel was able to effectively improve heart function and prevent myocardial apoptosis in the rat MI model.

## Discussion

In this work, we proposed a DNA hydrogel–based separation strategy that realized the specific and nondestructive separation of EXOs from complex biological media. The separation efficiency of $8 \times 10^7$ EXOs per 50 μL DNA hydrogel was achieved. For the release of EXOs from DNA hydrogel, two routes including enzymatic degradation and strand-displacement were demonstrated, and the released EXOs remained integrity of structure and composition. The applications of our DNA hydrogel were explored in the diagnosis of breast cancer and therapeutics of MI, achieving 100% precision for the detection of clinical breast cancer serum samples, and significant prevention of myocardial apoptosis in the rat MI model.

Notably, in our strategy, the DNA hydrogel that was formed by single-strand DNA chains was the key design to realize efficient separation and biomedical applications. First, although DNA chain on its own had the functions of recognizing and capturing EXOs, the DNA hydrogel format can encapsulate EXOs, which facilitated the separation of solid gel from liquid samples, without using specialized equipment and complicated operation. Second, during the formation of DNA hydrogel, EXOs that were captured by DNA chains can be efficiently enriched, increasing the local concentration of EXOs, and improving the sensitivity of detection.

We emphasize the expansibility of this DNA hydrogel–based separation technology in biomedical applications: 1) This technology is based on the high affinity between DNA aptamer with the target on EXOs. The programmability and molecular recognition ability of DNA molecules allow us to design the DNA hydrogel with different desired structures and functions to separate specific EXOs (12). 2) EXOs have shown application potential in clinical diagnosis and therapeutics (41, 42). The in situ-formed DNA hydrogel as the carrier of EXOs can easily achieve the separation of EXOs and change of medium. The nondestructive release ensures the high biological activity of EXOs. Consequently, this technology is conducive to the applications of EXOs in disease diagnosis and therapeutics. 3) The degradation time of DNA hydrogel can be extended and tuned by adding protective agents (43, 44). The enhanced DNA hydrogel can capture EXOs sustainably in the culture medium or in vivo and be utilized to block the cell–cell communication based on EXOs, which may be potential in the biomedical researches, such as tumor metastasis and recurrence. We envision that this DNA hydrogel–based separation technology is promising as a powerful biotechnology, which will promote the development of extracellular vesicles in biomedicine.

## Materials and Methods

**Rolling Circular Amplification (RCA).** In RCA system, circ-DNA (circ-DNA-1 and circ-DNA-2, respectively, 50 nmol/L), dNTPs (1 mmol/L) (TIANGEN, CD117), bovine serum albumin (0.2 mg/mL) (Solarbio, 9048-46-8), NaCl (80 mmol/L) (YUANLI, 7647-14-5), and phi29 polymerase (200 U/mL) [Biometa Life Science (Ningbo), BMT001L] were mixed in the buffer (50 mM Tris-HCl, 10 mM $MgCl_2$, 10 mM $(NH)_4SO_4$, 4 mM dithiothreitol, pH 7.5) [Biometa Life Science (Ningbo), BMT001L] and incubated at 37 °C, 450 rpm. Then the products were incubated at 65 °C for 10 min to inactivate phi29 polymerase. Two RCA products (DNA-chain-1 and DNA-chain-2) were mixed with equal volume at 37 °C, 450 rpm to form DNA hydrogel.

**Specificity of AptCD63 to EXOs.** In this experiment, the BMSC-derived EXOs were obtained by ultracentrifugation. The protein concentration of EXOs was measured by the BCA protein quantification kit (Yeasen, 20201ES76*). EXOs with protein concentration of 0.3 mg/mL were stained by 3 μM CM-DiI (Yeasen, 40718ES50) at 37 °C, 450 rpm for 30 min. Then, the EXOs were incubated with 0.1 μM FAM-labeled AptCD63 and FAM-labeled NC for 30 min at 37 °C, respectively. The samples were observed by using an inverted fluorescence microscope (Nikon, Ti-E).

**Encapsulation of EXOs by DNA Hydrogel.** In this experiment, the BMSC EXOs were obtained by ultracentrifugation. DNA-chain-1 (SYBR Green I staining) was incubated with EXOs (CM-DiI staining) at 37 °C for 30 min. DNA-chain-2 was then added and continued to be mixed at 37 °C for 30 min. The captured EXOs and hydrogel were observed by using a fluorescence microscope (Nikon, Ti-E).

**EXO Release by Enzymatic Cleavage.** DNA hydrogel was degraded by DNase I (Beyotime, BYT-D7073) with different concentration. The degradation rate of DNA hydrogel was calculated by measuring the ssDNA concentration in supernatant with a microvolume spectrophotometer (Quawell, Q5000).

**EXO Release by Strand Displacement.** The BMSC EXOs were obtained by ultracentrifugation. In PAGE test, three DSs (10 μM) were mixed with equal amounts (molar quantity) of AptCD63 and AptCD63+EXOs at 37 °C for 30 min under 1.25 mM $Mg^{2+}$, respectively. In fluorescence microscopy imaging, $DS_{32}$ was added in DNA hydrogel and incubated at 37 °C for 30 min to release EXOs. The final concentration of $DS_{32}$ was 2.5 μM. The displacement effect was observed by using an inverted fluorescence microscope (Nikon, Ti-E).

**Specificity of MB to miRNA.** Four Cy3-labeled MBs (MB-21, MB-27a, MB-375 and MB-NC) (100 nM) were mixed with three synthetic miRNAs (miR-21, miR-27a, and miR-375, 100 nM) at 37 °C, 450 rpm for 30 min, respectively. The fluorescence intensities of samples were measured by using a microplate reader (BioTek, SYNERGY H1). Excitation/emission: 530 nm/570 nm.

**Specificity of MB-21 to Exosomal miRNAs.** In this experiment, MCF-7 cells were cultured in complete DMEM-H media for 48 h, and the media were then treated by gradient centrifugation at 2,000 × g for 10 min, 10,000 × g for 30 min. In a 100 μL system, 10 μL media were mixed with 100 nM Cy3-labeled MB-21 at 37 °C for 30 min. Cy3-labeled MB-NC was used as control to be mixed with media. The fluorescence intensities of samples were measured by using a microplate reader (BioTek, SYNERGY H1). Excitation: 500 nm; emission: 530 to 600 nm.

**Detection of Exosomal miR-21 by DNA Hydrogel.** In this experiment, the cells (including MCF-7, MDA-MB-231 and BEAS-2B) were cultured in complete cell media for 48 h, and the media were then treated by gradient centrifugation at 2,000 × g for 10 min, 10,000 × g for 30 min. DNA-chain-1 and DNA-chain-2

were synthesized by RCA for 4 h. Phi29 polymerase was inactivated at 65 °C for 10 min. Cy3-labeled MB-21 (final concentration, 100 nM) and FAM-labeled SP (final concentration, 60 nM) were added into DNA-chain-1 and incubated at 37 °C, 450 rpm for 15 min. Then, 7 μL medium was added in 100 μL DNA-chain-1 and incubated at 37 °C, 450 rpm for 30 min. Next, 100 μL DNA-chain-2 was added and incubated at 37 °C, 450 rpm for 30 min to form DNA hydrogel. DNA hydrogel was washed once by PBS buffer. The green fluorescence and red fluorescence of DNA hydrogel were observed by using an inverted fluorescence microscope (Nikon, TI-E). The parameters were consistent under the same channel.

**Clinical Serum Sample Detection.** The clinical serum samples gradually melted by gradient warming. DNA-chain-1 and DNA-chain-2 were synthesized by RCA for 4 h. Phi29 polymerase was inactivated at 65 °C for 10 min. Cy3-labeled MB-21 (final concentration, 100 nM) and FAM-labeled SP (final concentration, 60 nM) were added into DNA-chain-1 and incubated at 37 °C, 450 rpm for 15 min. Then, the 10 μL of clinical serum sample was added to 100 μL of DNA-chain-1 and incubated at 37 °C, 450 rpm for 30 min. The 100 μL of DNA-chain-2 was added and incubated at 37 °C, 450 rpm for 30 min to form DNA hydrogel. DNA hydrogel was washed once by PBS buffer. The green fluorescence and red fluorescence of DNA hydrogels were observed by using an inverted fluorescence microscope (Nikon, TI-E). The parameters were consistent under the same channel.

**Echocardiography.** All rats were measured by transthoracic echocardiography under anesthesia after 4 wk by ultrasound imaging system (VisualSonics, Vevo 2100). Hearts were imaged 2D in long-axis views at the level of the greatest left ventricular diameter. LVEF and LVFS were determined by measurement from views taken from the infarcted area.

**Masson Trichrome Staining.** All rats were sacrificed after treatments for 4 wk. Hearts were harvested and stored in 4% paraformaldehyde (Solarbio, P1110). The paraffin sections of these hearts were treated by Masson's trichrome stain kit (Solarbio, G1340). Image analysis was performed with ImageJ software.

**TdT-Mediated dUTP Nick-End Labeling.** The paraffin sections of rat hearts were treated by the TUNEL apoptosis detection kit (Alexa Fluor 488) (Yeasen, 40307ES20*).

**Data, Materials, and Software Availability.** All study data are included in the article and/or *SI Appendix*.

**ACKNOWLEDGMENTS.** This work was supported in part by National Natural Science Foundation of China (Grant Nos.: 22225505, 22174097).

Author affiliations: [a]Frontiers Science Center for Synthetic Biology, Key Laboratory of Systems Bioengineering (Ministry of Education), Institute of Biomolecular and Biomedical Engineering, School of Chemical Engineering and Technology, Tianjin University, Tianjin 300350, P. R. China; and [b]Tianjin Medical University Cancer Institute and Hospital, Tianjin 300060, P. R. China

1. M. Mathieu, L. Martin-Jaular, G. Lavieu, C. Thery, Specificities of secretion and uptake of exosomes and other extracellular vesicles for cell-to-cell communication. *Nat. Cell Biol.* **21**, 9–17 (2019).
2. R. Kalluri, V. S. LeBleu, The biology, function, and biomedical applications of exosomes. *Science* **367**, eaau6977 (2020).
3. B. Liu *et al.*, Cardiac recovery via extended cell-free delivery of extracellular vesicles secreted by cardiomyocytes derived from induced pluripotent stem cells. *Nat. Biomed. Eng.* **2**, 293–303 (2018).
4. C. Liu *et al.*, Low-cost thermophoretic profiling of extracellular-vesicle surface proteins for the early detection and classification of cancers. *Nat. Biomed. Eng.* **3**, 183–193 (2019).
5. S. Liu *et al.*, Treatment of infarcted heart tissue via the capture and local delivery of circulating exosomes through antibody-conjugated magnetic nanoparticles. *Nat. Biomed. Eng.* **4**, 1063–1075 (2020).
6. W. Zheng *et al.*, Diagnosis of paediatric tuberculosis by optically detecting two virulence factors on extracellular vesicles in blood samples. *Nat. Biomed. Eng.* **6**, 979–991 (2022).
7. A. Akbar, F. Malekian, N. Baghban, S. P. Kodam, M. Ullah, Methodologies to isolate and purify clinical grade extracellular vesicles for medical applications. *Cells* **11**, 186 (2022).
8. H. Shao *et al.*, New technologies for analysis of extracellular vesicles. *Chem. Rev.* **118**, 1917–1950 (2018).
9. J. Chen *et al.*, Review on strategies and technologies for exosome isolation and purification. *Front. Bioeng. Biotech.* **9**, 811971 (2022).
10. L. Wu *et al.*, Aptamer-based detection of circulating targets for precision medicine. *Chem. Rev.* **121**, 12035–12105 (2021).
11. C. Yao, J. Ou, J. Tang, D. Yang, DNA supramolecular assembly on micro/nanointerfaces for bioanalysis. *Acc. Chem. Res.* **55**, 2043–2054 (2022).
12. W. Tan, M. J. Donovan, J. Jiang, Aptamers from cell-based selection for bioanalytical applications. *Chem. Rev.* **113**, 2842–2862 (2013).
13. Y. Zhao *et al.*, Nucleic acids analysis. *Sci. China Chem.* **64**, 171–203 (2021).
14. J. Zheng *et al.*, Rationally designed molecular beacons for bioanalytical and biomedical applications. *Chem. Soc. Rev.* **44**, 3036–3055 (2015).
15. C. Yao *et al.*, Double rolling circle amplification generates physically cross-linked DNA network for stem cell fishing. *J. Am. Chem. Soc.* **142**, 3422–3429 (2020).
16. C. Liu *et al.*, Lambda-DNA- and aptamer-mediated sorting and analysis of extracellular vesicles. *J. Am. Chem. Soc.* **141**, 3817–3821 (2019).
17. C. Yao *et al.*, T lymphocyte-captured DNA network for localized immunotherapy. *J. Am. Chem. Soc.* **143**, 19330–19340 (2021).
18. P. Song *et al.*, DNA hydrogel with aptamer-toehold-based recognition, cloaking, and decloaking of circulating tumor cells for live cell analysis. *Nano Lett.* **17**, 5193–5198 (2017).
19. J. Tang, J. Ou, C. Zhu, C. Yao, D. Yang, Flash synthesis of DNA hydrogel via supramacromolecular assembly of DNA chains and upconversion nanoparticles for cell engineering. *Adv. Funct. Mater.* **32**, 2107267 (2022).
20. M. M. Ali *et al.*, Rolling circle amplification: A versatile tool for chemical biology, materials science and medicine. *Chem. Soc. Rev.* **43**, 3324–3341 (2014).
21. C. Yao, R. Zhang, J. Tang, D. Yang, Rolling circle amplification (RCA)-based DNA hydrogel. *Nat. Protoc.* **16**, 5460–5483 (2021).
22. J. Kowal *et al.*, Proteomic comparison defines novel markers to characterize heterogeneous populations of extracellular vesicle subtypes. *Proc. Natl. Acad. Sci. U.S.A.* **113**, E968–E977 (2016).
23. M. Mathieu *et al.*, Specificities of exosome versus small ectosome secretion revealed by live intracellular tracking of CD63 and CD9. *Nat. Commun.* **12**, 4389 (2021).
24. Y. Li *et al.*, Molecular identification of tumor-derived extracellular vesicles using thermophoresis-mediated DNA computation. *J. Am. Chem. Soc.* **143**, 1290–1295 (2021).
25. H. Zhang *et al.*, Identification of distinct nanoparticles and subsets of extracellular vesicles by asymmetric flow field-flow fractionation. *Nat. Cell Biol.* **20**, 332–343 (2018).
26. D. Suck, DNA recognition by DNase I. *J. Mol. Recognit.* **7**, 65–70 (1994).
27. R. Crescitelli, C. Lasser, J. Lotvall, Isolation and characterization of extracellular vesicle subpopulations from tissues. *Nat. Protoc.* **16**, 1548–1580 (2021).
28. F. G. Kugeratski *et al.*, Quantitative proteomics identifies the core proteome of exosomes with syntenin-1 as the highest abundant protein and a putative universal biomarker. *Nat. Cell Biol.* **23**, 631–641 (2021).
29. R. Xu *et al.*, Extracellular vesicles in cancer–Implications for future improvements in cancer care. *Nat. Rev. Clin. Oncol.* **15**, 617–638 (2018).
30. Q. Fan *et al.*, The emerging role of exosome-derived non-coding RNAs in cancer biology. *Cancer Lett.* **414**, 107–115 (2018).
31. B. N. Hannafon *et al.*, Plasma exosome microRNAs are indicative of breast cancer. *Breast Cancer Res.* **18**, 90 (2016).
32. J. H. Lee, J. A. Kim, S. Jeong, W. J. Rhee, Simultaneous and multiplexed detection of exosome microRNAs using molecular beacons. *Biosens. Bioelectron.* **86**, 202–210 (2016).
33. J. Zhao *et al.*, Thermophoretic detection of exosomal microRNAs by nanoflares. *J. Am. Chem. Soc.* **142**, 4996–5001 (2020).
34. A. Bigdeli *et al.*, Ratiometric fluorescent nanoprobes for visual detection: Design principles and recent advances–A review. *Anal. Chim. Acta* **1079**, 30–58 (2019).
35. J. H. Lee, J. A. Kim, M. H. Kwon, J. Y. Kang, W. J. Rhee, In situ single step detection of exosome microRNA using molecular beacon. *Biomaterials* **54**, 116–125 (2015).
36. S. A. Melo *et al.*, Cancer exosomes perform cell-independent microRNA biogenesis and promote tumorigenesis. *Cancer Cell* **26**, 707–721 (2014).
37. Y. Xia *et al.*, A ratiometric fluorescent bioprobe based on carbon dots and acridone derivate for signal amplification detection exosomal microRNA. *Anal. Chem.* **90**, 8969–8976 (2018).
38. S. Sahoo, D. W. Losordo, Exosomes and cardiac repair after myocardial infarction. *Circul. Res.* **114**, 333–344 (2014).
39. H. Hashimoto, E. N. Olson, R. Bassel-Duby, Therapeutic approaches for cardiac regeneration and repair. *Nat. Rev. Cardiol.* **15**, 585–600 (2018).
40. L. Chen, A. Endler, F. Shibasaki, Hypoxia and angiogenesis: Regulation of hypoxia-inducible factors via novel binding factors. *Exp. Mol. Med.* **41**, 849–857 (2009).
41. L. Min *et al.*, Advanced nanotechnologies for extracellular vesicle-based liquid biopsy. *Adv. Sci.* **8**, 2102789 (2021).
42. L. S. Cheng, A. F. Hill, Therapeutically harnessing extracellular vesicles. *Nat. Rev. Drug. Discov.* **21**, 379–399 (2022).
43. A. R. Chandrasekaran, Nuclease resistance of DNA nanostructures. *Nat. Rev. Chem.* **5**, 225–239 (2021).
44. F. M. Anastassacos, Z. Zhao, Y. Zeng, W. M. Shih, Glutaraldehyde cross-linking of oligolysines coating DNA origami greatly reduces susceptibility to nuclease degradation. *J. Am. Chem. Soc.* **142**, 3311–3315 (2020).